

Comparing absorption from classic tracers of the diffuse interstellar medium at optical and radio wavelengths along the same sightlines

H. Liszt¹

National Radio Astronomy Observatory, 520 Edgemont Road, Charlottesville, VA, USA 22903 e-mail: hliszt@nrao.edu

received May 3, 2021

ABSTRACT

Aims. To compare information gained from radio and optical absorption line profiles from the diffuse interstellar medium along the same sightline

Methods. We compare new and existing $\lambda 21\text{cm}$ HI and $\lambda 3.4\text{mm}$ HCO⁺ profiles with profiles of the optical tracers CaII, NaI, and KI from an unpublished thesis of Tappe (2004)

Results. The atoms traced optically are all heavily depleted compared to a Solar abundance and only the integrated optical depths of HI and HCO⁺ correlate well with E(B-V). HCO⁺ is the species with by far the most limited kinematic distribution and the narrowest lines followed in order by KI, HI, NaI and CaII. CaII behaves separately in both column density and kinematics because it samples broader-lined warmer gas. Tracers of the cold neutral medium NaI, KI, HI and HCO⁺ share the same kinematic space statistically without correlating to nearly the same extent in abundance. N(NaI) and N(KI) are correlated, as are the integrated optical depths of HI and HCO⁺, but abundance correlations between optical and radio tracers are not seen. In the only direction with a measured CH⁺ profile, a 2 km s⁻¹ velocity shift between CH⁺ and CH, usually interpreted as the sign of shocked gas, is mimicked in the shift of HI relative to HCO⁺. CH and HCO⁺ appear in the ratios N(CH)/N(HCO⁺) = 14.6 and 21.1 along the two sightlines with optically-measured N(CH), compared with a mean of 12 determined previously at radio and submillimeter wavelengths.

Key words. interstellar medium – abundances; Chamaeleon

1. Introduction - An origin story

Radio and optical astronomers study the diffuse interstellar medium in complementary ways but often talk past each other without recognizing the contributions of the other side of their discipline. For instance the authoritative review article “Diffuse Atomic and Molecular Clouds” (Snow & McCall 2006) does not mention the $\lambda 21\text{cm}$ HI line of neutral atomic hydrogen¹. The realization that polyatomic molecules had been studied in absorption in diffuse clouds at radio wavelengths for some time (Cox et al. 1988; Lucas & Liszt 1993) was treated with disbelief in a preliminary draft of (Snow & McCall 2006).

That said, Snow & McCall (2006) did eventually come around, and they noted one work that explicitly bridged the gap, in which Tappe & Black (2004) observed red-shifted atomic optical absorption lines against the optically bright, radio-loud quasar B2145+067 whose Galactic HCO⁺ absorption had previously been observed at mm-wavelengths by Lucas & Liszt (1996). Snow & McCall (2006) noted a forthcoming paper that never appeared, in which Tappe and Black were to discuss the Galactic optical absorption toward B2145+067. Inspired by the idea that it might be possible to compare profiles of $\lambda 21\text{cm}$ HI absorption with those of NaI and KI, we procured a copy of Tappe’s unpublished thesis (Tappe 2004) on EBay and found that results were reported for five sightlines in sufficient detail that a full accounting of the observations and a reconstruction of the optical line profiles was possible. In turn we completed the

complementary roster of $\lambda 21\text{cm}$ HI and 89 GHz J=1-0 HCO⁺ absorption spectra that allows the present discussion comparing a full panoply of Galactic optical and radio profiles, especially $\lambda 21\text{cm}$ HI, for the first time.

Section 2 summarizes the new and old observational material discussed here. Section 3 is a detailed comparison of the optical (CaII, NaI, KI, CH, and CH⁺) and radio (HI and HCO⁺) line profiles toward the five sightlines noted in Table 1. Section 4 is a summary and section 5 is a coda giving some pertinent details not considered germane in the Introduction.

2. Observations

2.1. Some conventions

In this work, the rubric HI is used to denote neutral atomic hydrogen following Bohlin et al. (1978). N(H) is the column density of H-nuclei in atomic and molecular form, $N(\text{H}) = N(\text{H I}) + 2N(\text{H}_2) + N(\text{H}^+)$. We denote the integrated optical depth of the $\lambda 21\text{cm}$ HI line as Υ_{HI} . Velocities presented with the spectra are measured with respect to the kinematic definition of the Local Standard of Rest. Optical reddenings E(B-V) are taken from the work of Schlegel et al. (1998) and these are converted to total hydrogen column densities as $N(\text{H}) = 8.3 \times 10^{21} \text{ E(B-V)} \text{ cm}^{-2} \text{ mag}^{-1}$ (Liszt 2014).

Send offprint requests to: H. S. Liszt

¹ To be fair it also does not discuss CaII, NaI or KI

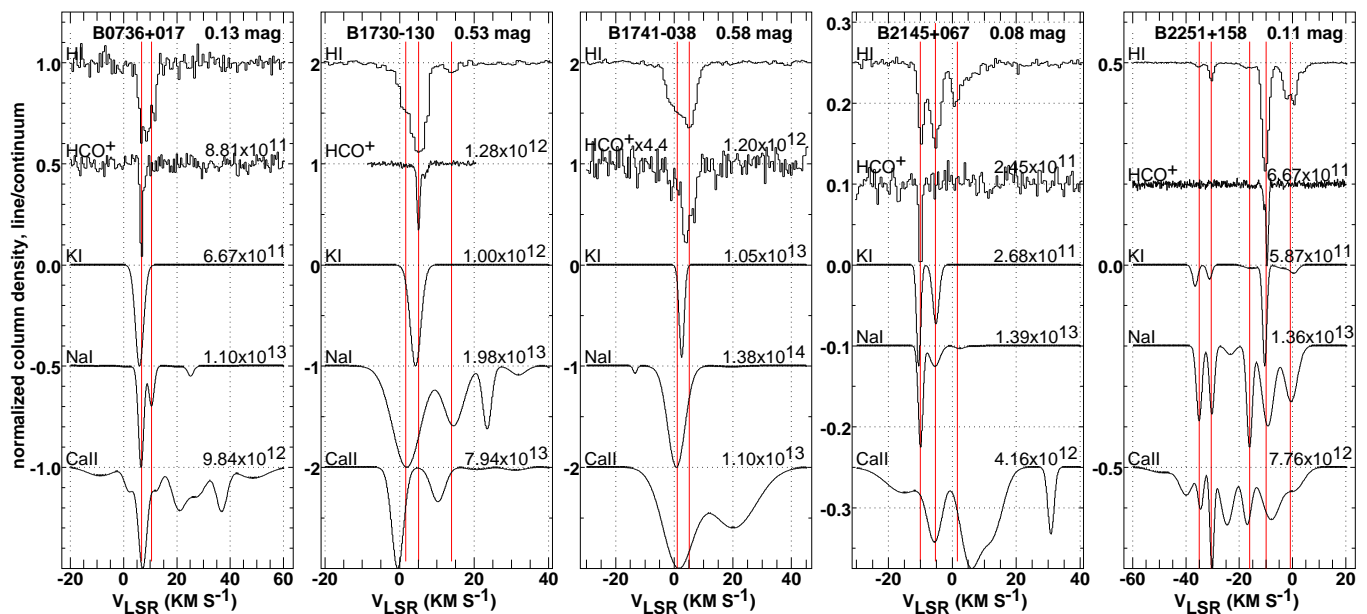


Fig. 1. Spectra of the optical and radio tracers for all sources. The HI and HCO⁺ spectra at the top in each panel are observed line/continuum ratios. Line profiles of the optical tracers KI, NaI and CaII are reconstructions of the gaussian decomposition of observed line profiles after deconvolution of the inherent atomic fine structure. The optical line profiles are in units of column density, inverted and scaled to fit the vertical scale. Total column densities of HCO⁺, KI, NaI and CaII are shown with each profile. E(B-V) values from Table 1 are shown for each source. Weak absorption from CaII, and occasionally from NaI, extends beyond the velocity range shown here.

Table 1. Sightline properties and abundances¹

Target	l deg	b deg	E(B-V) ² mag	N(CaII) log cm ⁻²	N(NaI) log cm ⁻²	N(KI) log cm ⁻²	N(CH ⁺) log cm ⁻²	N(CH) log cm ⁻²	N(HCO ⁺) log cm ⁻²	Υ_{HI} km s ⁻¹
B0736+017	216.990	11.380	0.129	12.977 (0.168)	13.045 (0.195)	11.824 (0.010)	13.145 (0.092)	13.113 (0.029)	11.949 (0.148)	3.203 (0.022)
B1730-130	12.032	10.812	0.526	13.900 (0.200)	13.296 (0.197)	12.000 (0.098)			12.106 (0.030)	10.927 (0.088)
B1741-038	21.591	13.127	0.579	13.043 (0.197)	14.140 (1.676)	13.020 (0.162)			12.079 (0.087)	8.146 (0.096)
B2145+067	63.656	-34.072	0.084	12.619 (0.662)	13.144 (0.748)	11.428 (0.162)			11.332 (0.249)	0.938 (0.014)
B2251+158	86.111	-38.184	0.108	12.890 (0.359)	13.134 (0.313)	11.769 (0.313)	<12.360	12.853 (0.161)	11.529 (0.020)	1.806 (0.018)
mean			0.285	13.35	13.59	12.41			11.89	5.00
mean ³			0.212	13.37	13.16	11.79			11.83	4.22
mean ⁴			0.118	12.94	13.09	11.80		13.00	11.79	2.50

¹Quantities in parentheses are the standard deviation of the value immediately above ²Schlegel et al. (1998) ³Omitting B1741-038 ⁴For sources with measured N(CH)

2.2. Optical absorption measurements and line profiles

Tappe (2004) measured optical absorption spectra of CaII, NaI, and KI toward the five compact extragalactic mm-wave continuum sources listed in Table 1 using the UVES instrument on the VLT, and observed CH and CH⁺ toward two sources, detecting CH⁺ in one case. The total column densities for these species given in Table 1 are taken directly from Tappe (2004) who deconvolved the atomic fine structure from his profiles and gave tables of Gaussian components fitting the deconvolved profiles. We reproduce Tappe's spectra in Figures 1 and 3 as the sum of these components rendered at 0.2 km s⁻¹ intervals. The optical profiles are presented in units of column density and inverted for comparison with the radiofrequency HI and HCO⁺ absorption spectra that are shown as observed line/continuum ratios. The optical spectra are arbitrarily normalized to fit the vertical scale in Figures 1 and 3 but column densities are shown with

the spectra in Figure 1. Sources with large column densities of a species tend to have fewer apparent features in the optical profiles shown here because higher total column densities are typically produced by one component that is so much stronger than others that the weaker lines are scarcely visible.

The NaI and KI column densities determined by Tappe (2004) toward B1741-038 are discrepant (see Figure 2) and have very large or undetermined errors, respectively (Table 1). These values receive special treatment in Table 1 and as noted in the discussion below when appropriate.

2.3. Radiofrequency absorption measurements of HI

λ 21cm HI profiles toward B1730-130 and B1741-038 were taken by Dickey et al. (1983). The appearance of Tappe (2004) spurred us to take HI profiles of the other sources at the eVLA

as previously presented in Liszt & Pety (2012) for all of the sources discussed here except B1741-038. Liszt & Pety (2012) also showed maps of CO $J=1-0$ emission in sky fields around the background sources except B1741-038.

2.4. Radiofrequency absorption measurements of HCO^+

Lucas & Liszt (1996) observed HCO^+ toward all the sources discussed here, and improved profiles were subsequently acquired at the PdBI instrument toward B1730-130 and B2251+158. Excitation temperatures are known to be very small in HCO^+ in diffuse molecular gas, given the weakness of emission that accompanies even very heavily saturated absorption lines (Lucas & Liszt 1996; Liszt 2020). We convert observed integrated HCO^+ optical depths to HCO^+ column density for a permanent dipole moment of 3.89 Debye assuming rotational excitation in equilibrium with the cosmic microwave background, i.e. $N(\text{HCO}^+) = 1.12 \times 10^{12} \text{ cm}^{-2} \int \tau(\text{HCO}^+) dv$.

2.5. Abundances of CH and HCO^+ relative to H_2

The abundances of CH and OH relative to H_2 have been measured on many sightlines with the results that $N(\text{CH})/N(\text{H}_2) = 3.6 \pm 0.8 \times 10^{-8}$ (Liszt 2007; Sonnentrucker et al. 2007; Sheffer et al. 2008; Weselak et al. 2009, 2010) and $N(\text{OH})/N(\text{H}_2) = 1.0 \pm 0.3 \times 10^{-7}$ (Weselak et al. 2009, 2010). In turn the $N(\text{HCO}^+)/N(\text{OH})$ and $N(\text{HCO}^+)/N(\text{CH})$ ratios have been measured at radio/submm wavelengths (Liszt & Lucas 1996; Gerin et al. 2019) with the result that $N(\text{HCO}^+)/N(\text{H}_2) = 3 \times 10^{-9}$ with an estimated uncertainty of ± 0.2 dex.

The observations discussed here are the first cases where CH has been detected in the optical waveband in directions with measured mm-wave HCO^+ absorption.

3. Observational results

General properties of the sightlines discussed here are given in Table 1, along with the integrated optical depths Υ_{HI} of HI and total column densities of the other tracers. Profiles for all sources are shown in Figure 1. Figure 2 plots total column densities and Υ_{HI} against $E(\text{B-V})$, Υ_{HI} , $N(\text{NaI})$ and $N(\text{HCO}^+)$.

3.1. Abundances, depletions, correlations with $E(\text{B-V})$ cum $N(\text{H})$

Table 2 shows the percentages of a Solar abundance (Lodders et al. 2009) that are represented by the total column densities of CaII, NaI and KI when $N(\text{H}) = 8.3 \times 10^{21} \text{ E}(\text{B-V}) \text{ cm}^{-2} \text{ mag}^{-1}$ (Liszt 2014). The fractional elemental abundances of sodium, calcium and potassium are small, at most $\approx 1\%$, and vary by factors of 7-8 among the various sightlines. If the dominant ion stage is being observed in each case, the small, sharply varying fractional abundances must reflect strong and heavily variable elemental depletion along moderately-reddened sightlines.

3.2. Correlations between abundances

The results shown in Figure 2 for the profile-integrated quantities are abstracted in a matrix of Pearson two-point r -function correlations in Table 3, where values with at least 3σ significance are shown in bold. The NaI and KI column densities determined toward B1741-038 were not included in this calculation owing to

their aberrant behavior (Figure 2). For such a small sample only very high degrees of correlation have even formal statistical significance. Nonetheless the spectral line tracers seem quite tribal; NaI correlates only with KI, and HCO^+ with H I.

$E(\text{B-V})$ is a measure of the bulk column density and all tracers are expected to be at least somewhat correlated with $E(\text{B-V})$ due to general mixing of conditions along the line of sight. The previously-demonstrated tight correlation of Υ_{HI} and $E(\text{B-V})$ (Liszt 2019) is strongly manifested even in this small sample. Given the known variability of the molecular gas fraction², it is perhaps surprising that $N(\text{HCO}^+)$ is better correlated with $E(\text{B-V})$ than are any of the optical atomic gas tracers. Apparently, elemental depletion and ionization equilibrium affect the optical atomic gas tracers to a greater extent than HI and HCO^+ are affected by the influences on their detectability - the H_2 fraction and ion molecule chemistry for $N(\text{HCO}^+)$, the kinetic temperature and phase equilibrium for $N(\text{HI})$ and Υ_{HI} .

The total abundances of NaI and KI are strongly coupled, despite some obvious kinematic disparities in Figure 1, and uncorrelated with that of CaII. Given its wider kinematic distribution, CaII will sample the warm and intercloud gas to a greater extent than any of the other tracers, but CaII is also the optical species best correlated with Υ_{HI} that avoids warmer gas. This is presumably a bulk effect of a high degree of mixing in the ISM.

Seeing the relationship of HI absorption to that of the canonical optical tracers was one of the most eagerly-anticipated results of this work. Despite the expectation of a dominant contribution from the atomic cold neutral medium (CNM) to NaI and KI, it is CaII and HCO^+ whose column densities are best correlated with Υ_{HI} . This is somewhat in contradiction to the kinematics on display in Figure 1 as quantified next.

3.3. Kinematics and kinematic correlations

HCO^+ is the species with by far the most limited kinematic distribution and the narrowest lines in Figure 1, followed in order by KI, HI, NaI and CaII. To quantify the comparison of line profiles we interpolated H I, HCO^+ and the optical atomic tracers toward each source onto a common velocity grid and calculated a kinematic correlation coefficient $r_k[m, n]$ between species m and n observed toward source k as

$$r_k[m, n] \equiv \int \hat{x}_m(v) \cdot \hat{x}_n(v) dv \quad 1$$

where $\hat{x}_m(v)$ and $\hat{x}_n(v)$ are the mean-subtracted column density (for optical tracers) or optical depth profiles of tracers m and n toward source k , expressed as vectors with unit maxima, equivalent to the Pearson two-point correlation functions shown in Table 3. This calculation used the profiles shown in Figure 1 and ignored some low column density features outside the velocity range shown, which appear mostly in CaII and less often in NaI. Normalizing each profile mitigates the influence of correlations and uncertainties in abundance and on this account we included the NaI and KI profiles toward B1741-038 in this calculation. Table 4 presents a matrix of the mean and standard deviation of this coefficient averaged over all directions k for the five tracers represented in Table 3. Values above the 3σ level are again shown in bold.

A complete dearth of kinematic correlations above the 3σ level shows that CaII occupies a different kinematic space from the other tracers, although only narrowly for NaI. By contrast,

² see for instance Figure 1 of Liszt et al. (2010)

the other tracers sampling the CNM and diffuse molecular gas all overlap significantly.

The KI profile is dominated by one strong component that overlaps with HCO^+ for the three sightlines having the highest molecular column densities (B0736, B1730, B1741). About one-third of the KI column density does not coincide with HCO^+ toward B2145 and B2251, as manifested in several kinematic components that presumably represent the tail of high atomic abundance at small $N(\text{H}_2)$ shown by Welty & Hobbs (2001) and discussed in Sect. 3.5 here. The same behaviour is exaggerated in NaI except toward B2145.

3.4. Optical CH and CH^+ vs radio HI and HCO^+

Figure 3 plots spectra of CH, CH^+ , HCO^+ and HI. The displacement between CH and CH^+ toward B0736 that is sometimes interpreted as the sign of a slow shock (Elitzur & Watson 1980; Monteiro et al. 1988; Flower & Pineau Des Forêts 1998) is intriguingly mimicked in HI. The eccentricity of HCO^+ with respect to the HI profile toward B2251 is typical (Liszt & Lucas 1996; Liszt & Pety 2012) and CH is aligned with neither.

The $N(\text{CH})/N(\text{HCO}^+)$ ratios observed toward B0736 and B2251 are 14.6 and 21.1 ± 0.15 dex, as compared with the mean ratio 12 ± 0.2 dex implied by the discussion in Section 2.5 (Gerin et al. 2019). This is reflected in slightly different implied molecular hydrogen fractions from CH and HCO^+ in Table 3 but both CH and HCO^+ are consistent in indicating a higher molecular fraction toward B0736.

3.5. How well do NaI or KI trace H_2 ?

Welty & Hobbs (2001) showed that NaI and KI are well correlated with $N(\text{H}_2)$ for $N(\text{H}_2) \gtrsim 10^{20} \text{ cm}^{-2}$, with substantial tails of appreciable atomic abundance at $N(\text{H}_2) \lesssim 10^{19} \text{ cm}^{-2}$ and large scatter and a substantial fraction of sightlines with very low $N(\text{NaI})$ and/or $N(\text{KI})$ at $10^{19} \text{ cm}^{-2} \lesssim N(\text{H}_2) \lesssim 10^{20} \text{ cm}^{-2}$. A column density $N(\text{H}_2) = 10^{20} \text{ cm}^{-2}$ corresponds approximately to $N(\text{HCO}^+) = 3 \times 10^{11} \text{ cm}^{-2}$ and only the line of sight toward B2145+067 has such a small $N(\text{HCO}^+)$ in the cohort studied here. That being the case it might be expected that $N(\text{NaI})$ and $N(\text{KI})$ would correlate well with $N(\text{HCO}^+)$ but that is not the case in Table 3: These species only correlate in velocity space (Table 4).

In retrospect it seems that CH, not NaI or KI, should be used to trace H_2 in the optical waveband as discussed in Sect. 2.5.

4. Summary

Figure 1 shows the line profiles of the five species measured toward all five sources (Table 1): HI, HCO^+ , KI, NaI and CaII. HCO^+ has by far the most limited kinematic distribution and the narrowest lines followed in order in this regard by KI, HI, NaI and CaII. The atoms traced optically are all heavily depleted compared to a Solar abundance (Table 2). The only abundance measures that correlate well with $E(\text{B}-\text{V})$ are the integrated optical depths of HI and HCO^+ (Table 3).

CaII behaves separately in both column density and kinematics because it samples broader-lined warmer gas. Tracers of the cold neutral medium (NaI, KI, HI and HCO^+) share the same kinematic space statistically with overlaps of 60-70% (Table 4) without correlating nearly as well in abundance (Table 3). $N(\text{NaI})$ and $N(\text{KI})$ are correlated, as are the integrated opti-

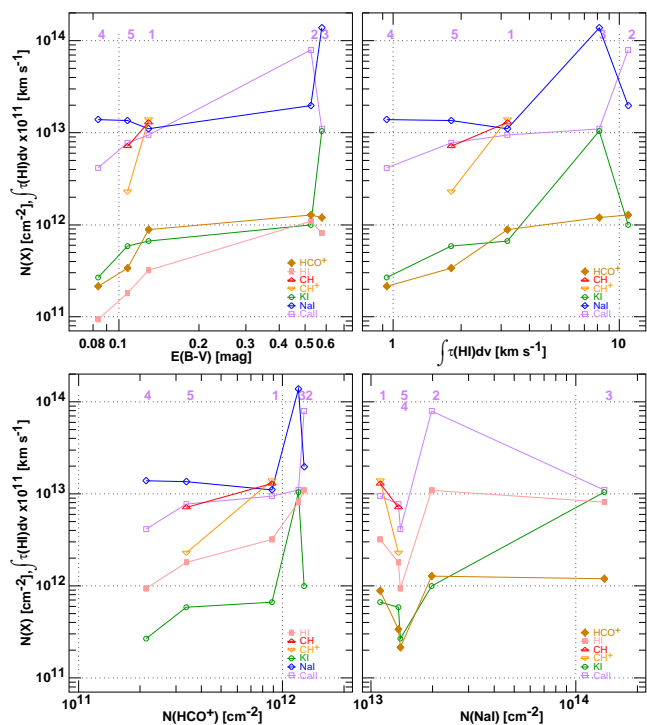


Fig. 2. Intercomparisons between $E(\text{B}-\text{V})$, Y_{HI} and measured column densities. Y_{HI} has been scaled upward by 10^{11} to appear on the same scale. The numerals at the top of each plot indicate which source's data is plotted at each abscissa, following the right ascension order in Table 1 and the left-right order in Figure 1.

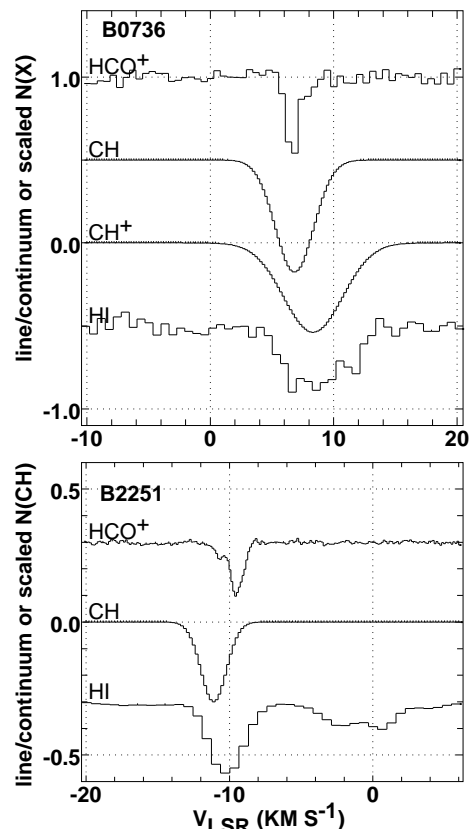


Fig. 3. Comparison of radio and optical molecular line profiles with HI. The vertical scale is as in Figure 1.

Table 2. Percentage fractional abundances

Source	CaII ¹	NaI ¹ %Solar	KI ¹	CH ² f _{H₂}	HCO ⁺ ³ f _{H₂}	HI ⁴ f _{HI}
B0736	0.41	0.52	0.47	67.16	55.03	32.63
B1730	0.85	0.23	0.17		19.46	27.37
B1741	0.11	1.44	1.65		16.62	18.56
B2145	0.28	1.01	0.29		20.58	14.78
B2251	0.41	0.76	0.50	44.30	25.13	22.08

¹Using $N(\text{H}) = 8.3 \times 10^{21} \text{ E(B-V) cm}^{-2} \text{ mag}^{-1}$ and Solar abundances from Lodders et al. (2009) ² $2N(\text{H}_2)/N(\text{H})$ if $N(\text{CH})/N(\text{H}_2) = 3.6 \times 10^{-8}$ ³ $2N(\text{H}_2)/N(\text{H})$ if $N(\text{HCO}^+)/N(\text{H}_2) = 3.0 \times 10^{-9}$ ⁴ $N(\text{HI})/N(\text{H})$ when $T_{\text{sp}} = 60 \text{ K}$

cal depths of HI and HCO⁺, but abundance correlations between optical and radio tracers are not seen in Table 3.

Four of the five sightlines have an NaI feature that is not matched in HI and only toward B2145 is there a feature (the highest velocity) in HI that is not matched in NaI. There are a few cases of HI features without KI counterparts in Figure 1, ie the highest velocity HI features toward B1730-130 and B2147+067 and perhaps the blue wings of the HI profiles toward B1730 and B1741, but no cases of KI features lacking a counterpart at some level in HI. KI is notably more broadly distributed than HCO⁺ toward B2145 and B2251, perhaps corresponding to a long-known tail of weak KI absorption at small N(H) and N(H₂) (see Section 3.5).

CH and HCO⁺ appear in the ratios $\log N(\text{CH})/N(\text{HCO}^+) = 1.2 \pm 0.15$ and 1.3 ± 0.16 along the two sightlines with measured N(CH) in Table 1, compared to an expected mean value of 1.1 ± 0.2 from other considerations discussed in Section 2.5, where the uncertainty considers only HCO⁺. In the only direction with a measured CH⁺ profile, a 2 km s⁻¹ velocity shift between CH⁺ and CH, usually interpreted as the sign of shocked gas, is intriguingly mimicked in the shift of HI relative to HCO⁺.

5. Coda

The origin story in the Introduction is a fabulist concoction (Frankfurt 2005). I did not need to procure a copy of Tappe (2004) on EBay because Achim Tappe and I were in touch when I provided some HCO⁺ spectra and explained how to use them while Achim was still a student. Unfortunately, neither this experience nor my subsequent prodding of the authors of Tappe & Black (2004) sufficed to elicit a paper describing the Galactic results. I subsequently completed the roster of HI and HCO⁺ spectra, allowing the present bagatelle.

Acknowledgements. The National Radio Astronomy Observatory is a facility of the National Science Foundation operated under cooperative agreement by Associated Universities, Inc. I thank Evelyne Roueff for discussions of the early draft text of Snow & McCall (2006) at the Asilomar astrochemistry meeting in 2005.

References

- Bohlin, R. C., Savage, B. D., & Drake, J. F. 1978, ApJ, 224, 132
Cox, P., Güsten, R., & Henkel, C. 1988, A&A, 206, 108
Dickey, J. M., Kulkarni, S. R., Heiles, C. E., & Van Gorkom, J. H. 1983, Ap. J. Suppl. Ser., 53, 591
Elitzur, M. & Watson, W. D. 1980, ApJ, 236, 172
Flower, D. R. & Pineau Des Forêts, G. 1998, MNRAS, 297, 1182
Frankfurt, H. G. 2005, On Bullshit (Princeton; New Jersey: Princeton University Press)
Gerin, M., Liszt, H., Neufeld, D., Godard, B., Sonnentrucker, P., Pety, J., & Roueff, E. 2019, A&A, 622, A26

Table 3. Quantity correlation coefficients¹

	CaII	NaI	KI	HCO ⁺	HI	E(B-V)
CaII		0.03 (0.71)	0.02 (0.71)	0.63 (0.45)	0.81 (0.34)	0.60 (0.46)
NaI	0.03 (0.71)		0.99 (0.08)	0.30 (0.67)	0.30 (0.67)	0.48 (0.62)
KI	0.02 (0.71)	0.99 (0.08)		0.35 (0.66)	0.31 (0.67)	0.48 (0.62)
HCO ⁺	0.63 (0.45)	0.30 (0.67)	0.35 (0.66)		0.92 (0.22)	0.88 (0.28)
HI	0.81 (0.34)	0.30 (0.67)	0.31 (0.67)	0.92 (0.22)		0.95 (0.19)
E(B-V)	0.60 (0.46)	0.48 (0.62)	0.48 (0.62)	0.88 (0.28)	0.95 (0.19)	

¹Quantities in parentheses are the formal standard deviation of the value immediately above

Table 4. Mean kinematic correlation coefficients¹

	CaII	NaI	KI	HCO ⁺	HI
CaII		0.58 (0.22)	0.32 (0.22)	0.29 (0.25)	0.47 (0.21)
NaI	0.58 (0.22)		0.65 (0.14)	0.58 (0.19)	0.71 (0.08)
KI	0.32 (0.22)	0.65 (0.14)		0.58 (0.06)	0.72 (0.15)
HCO ⁺	0.29 (0.25)	0.58 (0.19)	0.58 (0.06)		0.66 (0.16)
HI	0.47 (0.21)	0.71 (0.08)	0.72 (0.15)	0.66 (0.16)	

¹Quantities in this table are the mean over all five sources of the kinematic correlation coefficient defined in Eqn 1 and quantities in parentheses are the standard deviation of that mean

- Liszt, H. 2014, ApJ, 780, 10
—, 2019, ApJ, 881, 29
Liszt, H. S. 2007, A&A, 476, 291
—, 2020, ApJ, 897, 104
Liszt, H. S. & Lucas, R. 1996, A&A, 314, 917
Liszt, H. S. & Pety, J. 2012, A&A, 541, A58
Liszt, H. S., Pety, J., & Lucas, R. 2010, A&A, 518, A45+
Lodders, K., Palme, H., & Gail, H. P. 2009, Landolt & Bornstein, 4B, 712
Lucas, R. & Liszt, H. S. 1993, A&A, 276, L33
—, 1996, A&A, 307, 237
Monteiro, T. S., Flower, D. R., Pineau Des Forets, G., & Roueff, E. 1988, MNRAS, 234, 863
Schlegel, D. J., Finkbeiner, D. P., & Davis, M. 1998, ApJ, 500, 525
Sheffer, Y., Rogers, M., Federman, S. R., Abel, N. P., Gredel, R., Lambert, D. L., & Shaw, G. 2008, ApJ, 687, 1075
Snow, T. P. & McCall, B. J. 2006, Ann. Rev. Astron. Ap., 44, 367
Sonnentrucker, P., Welty, D. E., Thorburn, J. A., & York, D. G. 2007, Ap. J. Suppl. Ser., 168, 58
Tappe, A. 2004, PhD thesis, Chalmers (Göteborg, Sweden)
Tappe, A. & Black, J. H. 2004, A&A, 423, 943
Welty, D. E. & Hobbs, L. M. 2001, Ap. J. Suppl. Ser., 133, 345
Weselak, T., Galazutdinov, G., Beletsky, Y., & Krelowski, J. 2009, A&A, 499, 783
Weselak, T., Galazutdinov, G. A., Beletsky, Y., & Krelowski, J. 2010, MNRAS, 402, 1991